Research Square

Preprints are preliminary reports that have not undergone peer review.
They should not be considered conclusive, used to inform clinical practice,
or referenced by the media as validated information.

Rapid and Accurate Microseismic Source Location in 3D Heterogeneous Media with Precomputed Travel-Time Grid interpolation and Stochastic Regularization

Ruo Jia
CCTEG China Coal Research Institute
Hao Qiu
qiuhaogeo@163.com

CCTEG China Coal Research Institute
Wen Li
CCTEG China Coal Research Institute
Dapeng Zhao
Tohoku University
Yuguang Lian
CCTEG China Coal Research Institute
Kai Qin
CCTEG China Coal Research Institute
Yang Xu
CCTEG China Coal Research Institute

Article

Keywords: Microseismic source location, Ill-posed inverse problem, Stochastic regularization, 3D heterogeneous media, Precomputed travel-time grid, Geiger method

Posted Date: June 4th, 2026

DOI: https://doi.org/10.21203/rs.3.rs-9745948/v1

License: This work is licensed under a Creative Commons Attribution 4.0 International License.
Read Full License

Additional Declarations: No competing interests reported.

Rapid and Accurate Microseismic Source Location in 3D Heterogeneous Media with Precomputed Travel-Time Grid interpolation and Stochastic Regularization

Ruo Jia[1,2], Hao Qiu[1,2]*, Wen Li[1]*, Dapeng Zhao[3], Yuguang Lian[1], Kai Qin[1], Yang Xu[1]

[1]*CCTEG China Coal Research Institute, Beijing 100013, China. Email: jljiaruo@outlook.com.*
[2]*State Key Laboratory of Digital Intelligent Technology for Unmanned Coal Mining, Beijing 100013, China.*
[3]*Department of Geophysics, Graduate School of Science, Tohoku University, Sendai 980-8578, Japan.*

Correspondence and requests for materials should be addressed to H.Q. (email: qiuhaogeo@163.com)

Abstract

Rapid and accurate microseismic source location is essential for safe mining operations and real-time hazard early warning. However, limited by the constrained observational geometries and strong anthropogenic noise in underground mines, the misfit function in conventional travel-time-based location methods often becomes severely ill-conditioned, making the inversion results extremely sensitive to observational errors. This problem is further exacerbated in three-dimensional (3D) heterogeneous media. To address these challenges, this study proposes an improved high-precision source location workflow suitable for 3D heterogeneous media, built upon the classical Geiger location framework. Integrating concepts from the stochastic process theory and random matrix theory, we develop a stochastic data perturbation regularization method. In this approach, an arrival-time window replaces the conventional single-pick as the data input, and multiple stochastically perturbed datasets are used to reformulate the misfit function, thereby reducing the sensitivity of the inversion system to data error perturbations. Furthermore, by precomputing grid fields of theoretical travel-times and partial derivative coefficients over the entire volume, the forward calculation is decoupled from the iterative inversion, substantially improving the source location efficiency in 3D heterogeneous media. Synthetic tests demonstrate that the proposed method leads to accurate and rapid location results for co-planar sensor arrays deployed along coal mine working face. For observed arrival-time data containing error perturbations in a range of [-4, +4] ms, a single-event location takes 1–2 s, and the mean source location error is less than 5 m when the event lies inside the network coverage. This method is applied to real microseismic monitoring data from the No. 2301 working face of the Zhaozhuang Coal Mine, China. The results show that the precisely located epicenters exhibit a distinct pattern of synchronous migration with the advance of the mining face, consistent with previous findings. These results indicate that the proposed method provides an efficient and robust tool for microseismic source location in limited mining observation settings.

Keywords Microseismic source location, Ill-posed inverse problem, Stochastic regularization, 3D heterogeneous media, Precomputed travel-time grid, Geiger method

Introduction

Rapid and accurate source location is a critical component of microseismic monitoring in mines. In coal mining settings, the spatiotemporal clustering of microseismicity is often closely associated with local stress concentrations and the propagation and instability of fractures[1]. Research in this field is of great significance for the prediction, prevention, and control of hazards such as rockbursts, roof falls, gas outbursts, and water inrushes[2]. At present, in practical engineering operations and hazard early warning, travel-time-based location techniques, represented by the Geiger method[3], remain the mainstream and most widely used in the majority of field applications. Compared with waveform-based approaches[4-7], the travel-time-based methods offer distinct computational advantages, which stem from their foundation on linear approximation based on Taylor expansion. However, taking coal mine microseismic monitoring as an example, seismic sensors are usually deployed along the gateways on two sides of the working face, forming a near-coplanar array (Fig. 1) and only P-wave arrivals could be identified due to a noisy environment. This limited observation condition often makes the linearized travel-time equations severely ill-conditioned, so the inversion result becomes extremely sensitive to errors in the observed arrival-time data. In addition, when applied to three-dimensional (3D) heterogeneous media, the traditional methods typically involve time-consuming forward calculations, which makes it difficult to achieve the real-time monitoring and early warning demanded by safe mining operations.

In underground mines, operational interference often introduces substantial picking errors in arrival times, directly compromising source location accuracy. An early systematic study on mining microseismic location[8] showed that an arrival-time deviation of only 0.1 ms can cause an average location error of 3–4 m. N. Li's study revealed a nearly linear relationship between picking errors and location errors, and demonstrated that an unfavorable array layout can significantly amplify this effect[9]. A field measurement at a coal mine shows that 1–3 ms arrival-time errors can lead to 50–100 m location errors[10]. Li *et al.*[11] studied the location accuracy for events outside a network, and found that, in the absence of outliers, the traditional method yielded errors of ~20 m when arrival-time data had small random errors of 2 ms. They further proposed that the VFOM method can effectively reduce the outlier effects. Zeng *et al.*[12] evaluated several location algorithms commonly used in mining areas and found that, with 5 ms observational errors, the average location errors ranged from 20 to 50 m.

Theoretically, in the Geiger-type location methods, the sensitivity of the inversion results to data errors is governed by the degree of ill-conditioning of the equations. Therefore, effectively reducing the condition number of the coefficient matrix is key to improving the location accuracy. The Tikhonov regularization technique[13] is often chosen as the first strategy toward this goal, which has been successfully implemented in a range of ill-posed optimal control problems[14–18]. This method augments the misfit function with a penalty term, thereby embedding prior information on the solution and balancing the trade-off between the data consistency and solution energy. The random matrix method[19] is also an effective tool for solving noisy linear inversion problem, which deduces the condition number of the system by using a stochastic linear matrix operator $\mathbf{A}'$ instead of the original matrix $\mathbf{A}$[20]. In addition, probabilistic location methods based on the Bayesian inversion[21,22] offer distinct advantages in handling data errors and quantifying the inversion uncertainty. However, due to the high computational cost of stochastic algorithms, their practical application to mine sites remains limited.

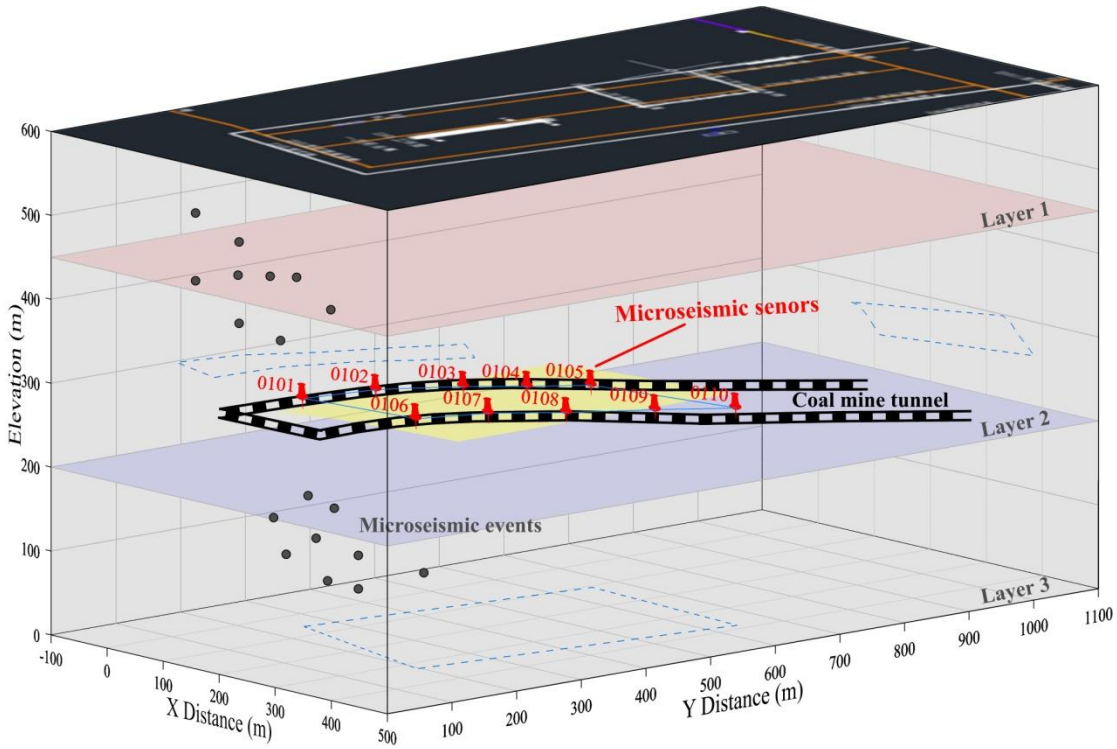


Figure 1. A microseismic monitoring array at the No. 2301 working face of the Zhaozhuang Coal Mine, China. The track lines represent coal mine roadways; the red markers denote ten microseismic sensors deployed along the roadways; the dark gray dots represent hypothetical microseismic events; the light blue dashed lines indicate projections of the monitoring network boundaries onto different coordinate planes.

To date, most commercial microseismic monitoring systems used in mines—such as the ESG system (Canada), the ARAMIS and SOS systems (Poland), the MicroSeismic system (USA), and the KJ series (China)—predominantly rely on homogeneous or layered velocity models. These models overlook complex 3D heterogeneous media, which would more closely represent the actual subsurface conditions in mining areas. Jia *et al.*[23] incorporated a 3D heterogeneous velocity model into the conventional Geiger linear inversion and showed that an accurate 3D model can effectively improve the location accuracy. Zhou *et al.*[24] further demonstrated the feasibility of constructing reliable 3D velocity models based on real geologic structures through synthetic tests and numerical experiments. However, incorporating a 3D model inevitably renders the source location problem more ill-conditioned and degrades computational efficiency. Even for the travel-time-based inversion methods rooted in ray theory, the computational performance of existing 3D ray tracing techniques remains inadequate to meet the real-time requirement of locating microseismic events within seconds in most mining areas. Therefore, developing faster 3D ray tracing algorithms, or decoupling the forward modeling from the inversion process, would be viable solutions.

Based on the above-mentioned findings, this study focuses on the microseismic source location problem under limited observational conditions—particularly the coplanar sensor arrays deployed along coal mine gateways with only P-wave data available (Fig. 1)—and seeks to develop a novel inversion workflow. This workflow is designed to address two core issues, namely, inversion sensitivity to data errors in an ill-conditioned system and rapid inversion in 3D

heterogeneous models, thereby meeting the demand for low-cost, real-time hazard monitoring and early warning at mine sites. To mitigate the inversion sensitivity to arrival-time errors, we propose a stochastic data perturbation regularization (SDPR) method. In this approach, an arrival-time window is used as input in place of a single arrival-time, and a quasi-Newton algorithm is then employed to achieve stable and rapid convergence. Furthermore, drawing on the idea of Bayesian inversion, we utilize multiple inversion results generated with different random datasets to estimate the final location errors. To address the problem of rapid inversion with a 3D velocity model, we adopt a strategy based on precomputed travel-time grid interpolation. First, for each seismic sensor, we precompute the theoretical travel-time field and the partial derivative coefficient fields at all grid nodes within the 3D domain. During inversion iterations, the theoretical travel-time at an arbitrary point is then obtained by interpolation. In this way, the time-consuming step of ray tracing can be decoupled from the iterative inversion process, substantially improving the real-time performance of the source location. Based on extensive synthetic tests, we verify that the proposed method can substantially mitigate the impact of data errors on source location results, even under limited observational conditions. For complex 3D heterogeneous media, the method simultaneously delivers high computational efficiency and location accuracy. We further applied the workflow to field data from the Zhaozhuang Coal Mine, and the results reveal a distinct pattern in which microseismic activity migrates synchronously with the direction of mining face advance, a finding that is consistent with the established empirical understanding.

Methods

(1) Stochastic data perturbation regularization

Based on a first-order Taylor expansion, given initial hypocentral parameters (x_0, y_0, z_0, t_0), the misfit function of the Geiger location method[3] in a Cartesian coordinate system is:

$$T_i^{\mathrm{obs}} - T_i^{\mathrm{cal}} = \Delta t + \left.\frac{\partial T_i^{\mathrm{cal}}}{\partial x}\right|_{(x_0,y_0,z_0,t_0)} \Delta x + \left.\frac{\partial T_i^{\mathrm{cal}}}{\partial y}\right|_{(x_0,y_0,z_0,t_0)} \Delta y + \left.\frac{\partial T_i^{\mathrm{cal}}}{\partial z}\right|_{(x_0,y_0,z_0,t_0)} \Delta z \quad (1)$$

where T_i^{obs}, T_i^{cal} are the observed and theoretical arrival-times at the ith seismic sensor, respectively. The matrix form is:

$$\mathbf{b} = \mathbf{A}\mathbf{m} \quad (2)$$

where

$$b_i = T_i^{\mathrm{obs}} - T_i^{\mathrm{cal}} \quad (3)$$

Under limited observational conditions—specifically, a co-planar array layout with only P-wave data available—the above system of equations often becomes severely ill-conditioned, making it difficult to obtain a stable solution. Tikhonov regularization[13] is commonly employed to address this issue:

$$\begin{bmatrix}\mathbf{b}\\ \mathbf{o}\end{bmatrix} = \begin{bmatrix}\mathbf{A}\\ \lambda\mathbf{I}_4\end{bmatrix}\mathbf{m} \quad (4)$$

However, many practical works have shown that when dealing with some special observation conditions and poor data quality, the location errors obtained from equation 4 are still relatively large, especially for the focal depths. Based on the stochastic process theory, Franklin[21] proposed a well-posted stochastic extension form of this problem. Drawing on this approach and incorporating ideas from random matrix theory[20], we further propose a stochastic data perturbation regularization method. The details of this method are as follows. For low-signal-to-noise-ratio

(low-SNR) microseismic data acquired in mining areas, instead of a single pick, a time window likely containing the accurate arrival-time is selected. Within this window, multiple sets of "perturbed" arrival-time data are generated by random sampling. These perturbed datasets are then used to construct corresponding systems of equations, and finally, a new misfit function is formulated based on all the perturbed datasets:

$$\mathbf{d} = \mathbf{G}\mathbf{m} \tag{5}$$

where

$$\mathbf{G} = \mathbf{W}\begin{bmatrix} \mathbf{A} \\ \mathbf{A} \\ \vdots \\ \mathbf{A} \\ \lambda\mathbf{I}_4 \end{bmatrix}$$

$$\mathbf{d} = \begin{bmatrix} \boldsymbol{\tau}_1 - \mathbf{T}^{\mathrm{cal}} \\ \boldsymbol{\tau}_2 - \mathbf{T}^{\mathrm{cal}} \\ \vdots \\ \boldsymbol{\tau}_N - \mathbf{T}^{\mathrm{cal}} \\ \mathbf{o} \end{bmatrix}, \boldsymbol{\tau}_j \in [\mathbf{l}, \mathbf{u}] \tag{6}$$

where $\boldsymbol{\tau}_1$,$\boldsymbol{\tau}_2$,…,$\boldsymbol{\tau}_N$ are random vectors taking values in the observed arrival-time interval [**l**, **u**]. **W** is weighting matrix. N is the selected total number of the perturbed datasets. Clearly, a larger N implies more comprehensive sampling and thus a more stable inversion result. However, the resulting increase in the size of the system of equations also leads to higher computational time and memory consumption. In this work, by performing a series of tests, we find that N=50 is suitable for the microseismic arrays of the Zhaozhuang Coal Mine, which contains 10 seismic sensors.

Based on the least-squares method, we get:

$$\min\|\mathbf{d} - \mathbf{G}\mathbf{m}\|_2 \tag{7}$$

This function could be solved by using a quasi-Newton optimization algorithm[25–27], which provides a fast second-order convergence. Then the optimal estimate $\mathbf{m}_{\mathrm{opt}}$ is used to update the hypocentral parameters, and a new Taylor expansion is carried out at the updated hypocentral location. The final hypocentral location is obtained after several iterations:

$$\begin{bmatrix} x_{k+1} \\ y_{k+1} \\ z_{k+1} \\ t_{k+1} \end{bmatrix} = \begin{bmatrix} x_k \\ y_k \\ z_k \\ t_k \end{bmatrix} + s * \mathbf{m}_{\mathrm{opt}} \tag{8}$$

where k is number of location iterations and s is iteration step. In each iteration, the $\mathbf{G}_k$ and $\mathbf{d}_k$ should be updated through forward calculation, which is time consuming when a 3D velocity model is considered. To address this issue, we further propose a forward and inversion separation technique based on ray theory.

(2) Precomputed travel-time grid interpolation

For 3D media, Julian[28] gave the ray perturbation formulation in Cartesian coordinates based on the ray-theoretical approximation as:

$$
\begin{aligned}
\frac{\mathrm{d}X}{\mathrm{d}t} &= v\cos\alpha \\
\frac{\mathrm{d}Y}{dt} &= v\cos\beta \\
\frac{\mathrm{d}Z}{\mathrm{d}t} &= v\cos\gamma \\
\frac{\mathrm{d}\alpha}{\mathrm{d}t} &= \frac{\partial v}{\partial X}\sin\alpha - \frac{\partial v}{\partial Y}\cot\alpha\cos\beta - \frac{\partial v}{\partial Z}\cot\alpha\cos\gamma \\
\frac{\mathrm{d}\beta}{\mathrm{d}t} &= -\frac{\partial v}{\partial X}\cos\alpha\cot\beta + \frac{\partial v}{\partial Y}\sin\beta - \frac{\partial v}{\partial Z}\cot\beta\cos\gamma \\
\frac{\mathrm{d}\gamma}{\mathrm{d}t} &= -\frac{\partial v}{\partial X}\cos\alpha\cot\gamma - \frac{\partial v}{\partial Y}\cos\beta\cot\gamma + \frac{\partial v}{\partial Z}\sin\gamma
\end{aligned}
\tag{9}
$$

where X, Y and Z are coordinates of the points on the ray path. v represents seismic velocity. Then, the partial derivative term of equation 1 is obtained:

$$
\begin{aligned}
\frac{\partial T}{\partial x} &= -\frac{1}{v}\cos\alpha_{\mathrm{o}} \\
\frac{\partial T}{\partial y} &= -\frac{1}{v}\cos\beta_{\mathrm{o}} \\
\frac{\partial T}{\partial z} &= -\frac{1}{v}\cos\gamma_{\mathrm{o}}
\end{aligned}
\tag{10}
$$

where $\alpha_{\mathrm{o}}, \beta_{\mathrm{o}}, \gamma_{\mathrm{o}}$ are direction angles of the tangent to the ray emitted from the hypocenter and can be obtained by ray tracing.

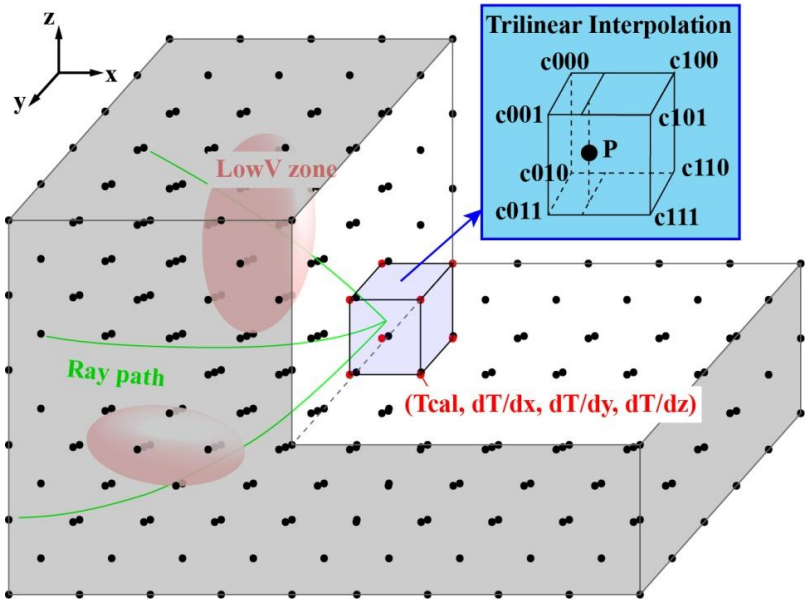


Figure 2. 3D schematic diagram of the precomputed travel-time grid interpolation method. The green lines denote ray paths. Two light pink ellipsoids represent possible velocity anomalies in the 3D medium. The theoretical travel-time (Tcal) and partial derivative coefficients (dT/dx, dT/dy, dT/dz) at any point are calculated using trilinear interpolation. For more details, see the main text.

Currently, the mainstream ray-tracing methods include the shooting method, the bending (and pseudo-bending) method, the fast marching method, the shortest path method, and finite-difference solutions of the eikonal equation. Although several improved fast ray-tracing methods[29,30] have achieved significant gains in computational efficiency, they are still unable to deliver second-level source location when the velocity model is complex. To address this issue, we propose an interpolation-based technique that decouples the forward calculation from the inversion. First, the target volume is discretized into a 3D grid of $n \times m \times l$ points, which are treated

as virtual sources. For each seismic sensor, the travel-time and the partial derivative coefficients with respect to each virtual source are then computed and stored as grid field data. During inversion, the theoretical travel-time and partial derivative coefficients required at any points in equation 1 are rapidly obtained via trilinear interpolation[31] by using the precomputed grid fields (Fig. 2). In this way, the time-consuming forward calculation is separated from the iterative inversion process, greatly improving the source location efficiency.

Note that this approach introduces numerical errors arising from interpolation, the magnitude of which is governed by the grid interval. Nevertheless, because the forward calculation and the inversion are mutually independent, a sufficiently fine grid can be adopted in practice to achieve high accuracy. An additional advantage of this method is its inherent adaptability to time-varying velocity models. However, since the forward computation of the travel-time field over the entire volume is inherently time-consuming, the updated interval for the velocity model cannot be arbitrarily short. As an illustration, under our test configuration—ten sensors with an inter-station distance of ~100 m, a grid comprising 300,000 nodes, and a 3D heterogeneous velocity model—one complete forward calculation using the shooting method required approximately 8–10 hours of wall-clock time with 12-core parallel computation.

Synthetic tests

To validate the effectiveness of our method, we performed a series of synthetic tests. The observation geometries are adopted from three seismic array deployments on the No. 2301 working face of the Zhaozhuang Coal Mine, each consisting of ten KJ768 microseismic sensors[32]. These arrays were installed on 27 July, 24 August, and 9 October 2024, and were progressively relocated northward as the mining face advanced (Fig. 3).

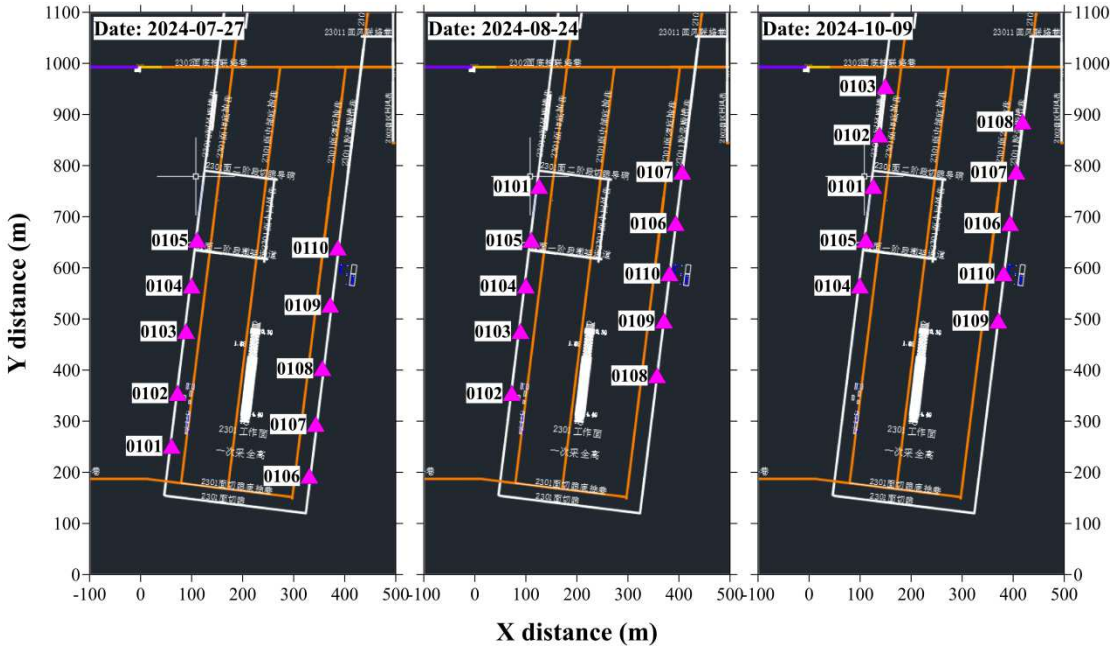


Figure 3. Distributions of three microseismic monitoring arrays at the No. 2301 working face of the Zhaozhuang Coal Mine. Purple triangles denote the KJ768 microseismic sensors. The base map is the mining engineering plan. The deployment dates of the three arrays are annotated at the upper-left corner of each map.

(1) Reliability test of the SDPR method

We first simulated two seismic events in a homogeneous medium. One is located inside the network coverage deployed on July 27, 2024 and the other is located outside the network. Three sets of random error perturbations, uniformly distributed in ranges of [-2, +2] ms, [-4, +4] ms, and [-6, +6] ms, are respectively added to the theoretical arrival-times for comparative analysis. Following the Bayesian framework for probabilistic source location, 100 datasets, each incorporating a different set of random error perturbations, are constructed to obtain the probability density function (PDF) of the source parameters. Only P-wave arrival-times are used in all the tests. Inversions are then conducted using both the conventional Tikhonov regularization and the proposed SDPR method as mentioned above. As shown in Figs 4–5 and S1–S12, the PDF obtained with the SDPR inversion is markedly sharper and exhibits a single, well-defined peak. For arrival-time data containing error perturbations within [-4, +4] ms, the conventional Tikhonov inversion yields a depth error of up to 100 m for events inside the network coverage and an origin time error exceeding ±5 ms (Fig. 4). In contrast, the SDPR inversion reduces the depth error to less than 5 m and keeps the origin time error within ±5 ms (Fig. 5). Outside the network coverage, the location accuracy degrades for both methods, but the SDPR results remain noticeably more stable, with a distinct PDF peak still observable (Figs S10–S12). Furthermore, our tests show that, under the array geometry and inversion settings used in this study (as described above), the SDPR method requires 1–2 s per event, which is slightly faster than the 1–3 s required by the conventional method. This improvement is largely due to the more stable and rapid convergence provided by the SDPR. Additional tests indicate that the overall shape of the spatial source location PDF remains stable regardless of whether the random error perturbations follow a one-sided or a two-sided symmetric distribution (Figs S5 and S6). This robustness stems from the fact that the error distribution is inherently random, whereas the useful signal carries a stable, trend-like signature. In summary, the proposed SDPR method offers clear advantages over the conventional approach in both location accuracy and computational efficiency, and it shows extremely low sensitivity to error perturbations in observed arrival-times. Notably, the SDPR inversion produces highly stable spatial source locations, which show extremely low sensitivity to the statistical properties of the data error distribution.

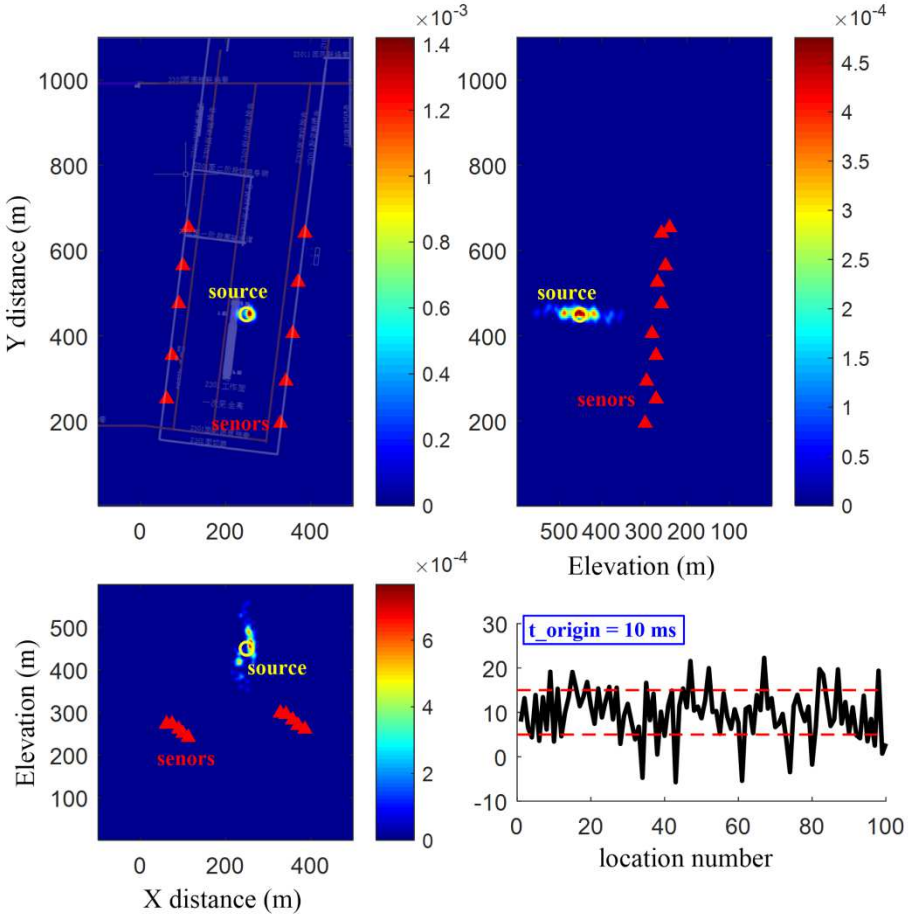


Figure 4. Source location probability density function from the synthetic tests. The conventional Tikhonov regularization method is used in the inversion. For the inversion, a total of 100 datasets are used, each incorporating random error perturbations uniformly distributed within [-4, +4] ms. The yellow open circle marks the true source location of the synthetic event. Red and blue colors indicate high- and low-probability regions, respectively. The inset at the lower-right corner shows the distribution of the inverted origin times obtained from the datasets. The true origin time is set to 10 ms; the black solid line represents the inversion results, and the red dashed lines delineate the ±5 ms error interval.

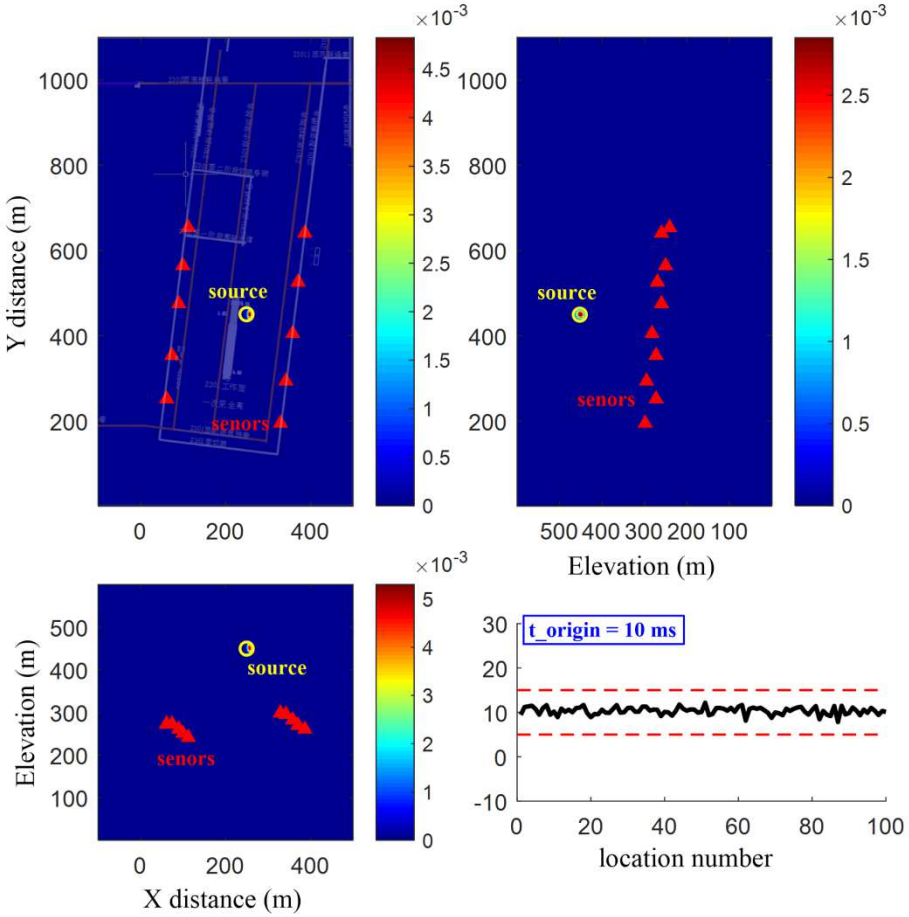


Figure 5. Same as Figure 4 but with the SDPR method for the inversion.

Furthermore, we generated 30,000 synthetic microseismic events within the roof area of the working face, with 500 events at each depth level (Figs S13–S15), where the depths are defined at elevation = 300, 350, 400, 450, 500, 550 m. These events are located using our proposed method with three array geometries deployed on 27 July, 24 August, and 9 October 2024. Random error perturbations uniformly distributed within [-5, +5] ms are added to the synthetic arrival-times, and a homogeneous velocity model is adopted. Figures 6–8 show the contours of absolute location errors on horizontal slices at six elevations for the three array geometries. As can be observed, as the arrays were progressively relocated northward, the zone of large errors shifted from being concentrated in the north on 27 July (Fig. 6) to being concentrated in the south by 9 October (Fig. 8). Further analysis reveals that, within the network coverage, most of the synthetic events are well located, with a mean spatial location error of less than 5 m and an origin time error of less than 5 ms (Figs S13–S15). Beyond ~100 m from the network coverage, the location accuracy gradually deteriorates, with most errors falling between 50 and 100 m (Figs 6–8).

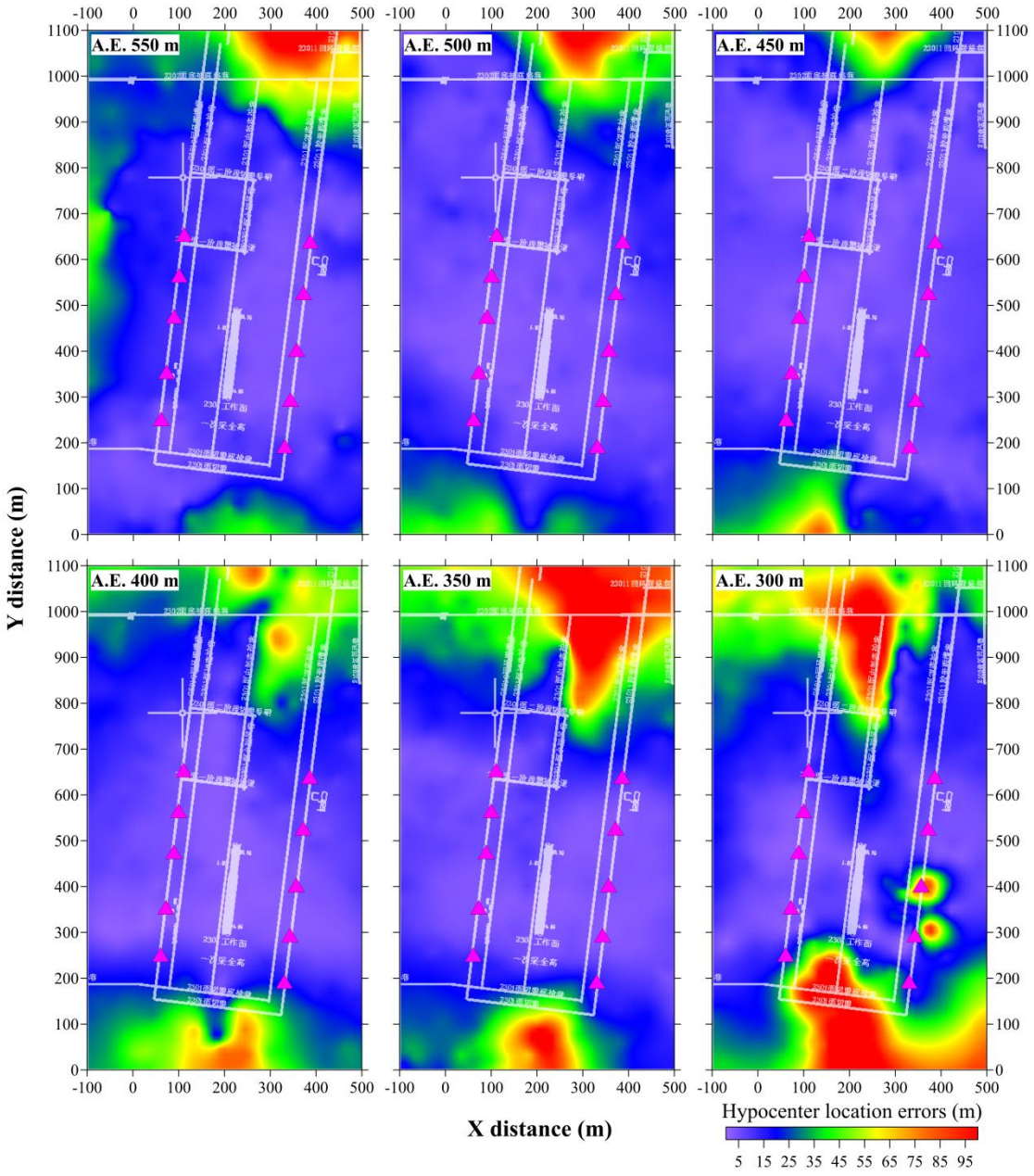
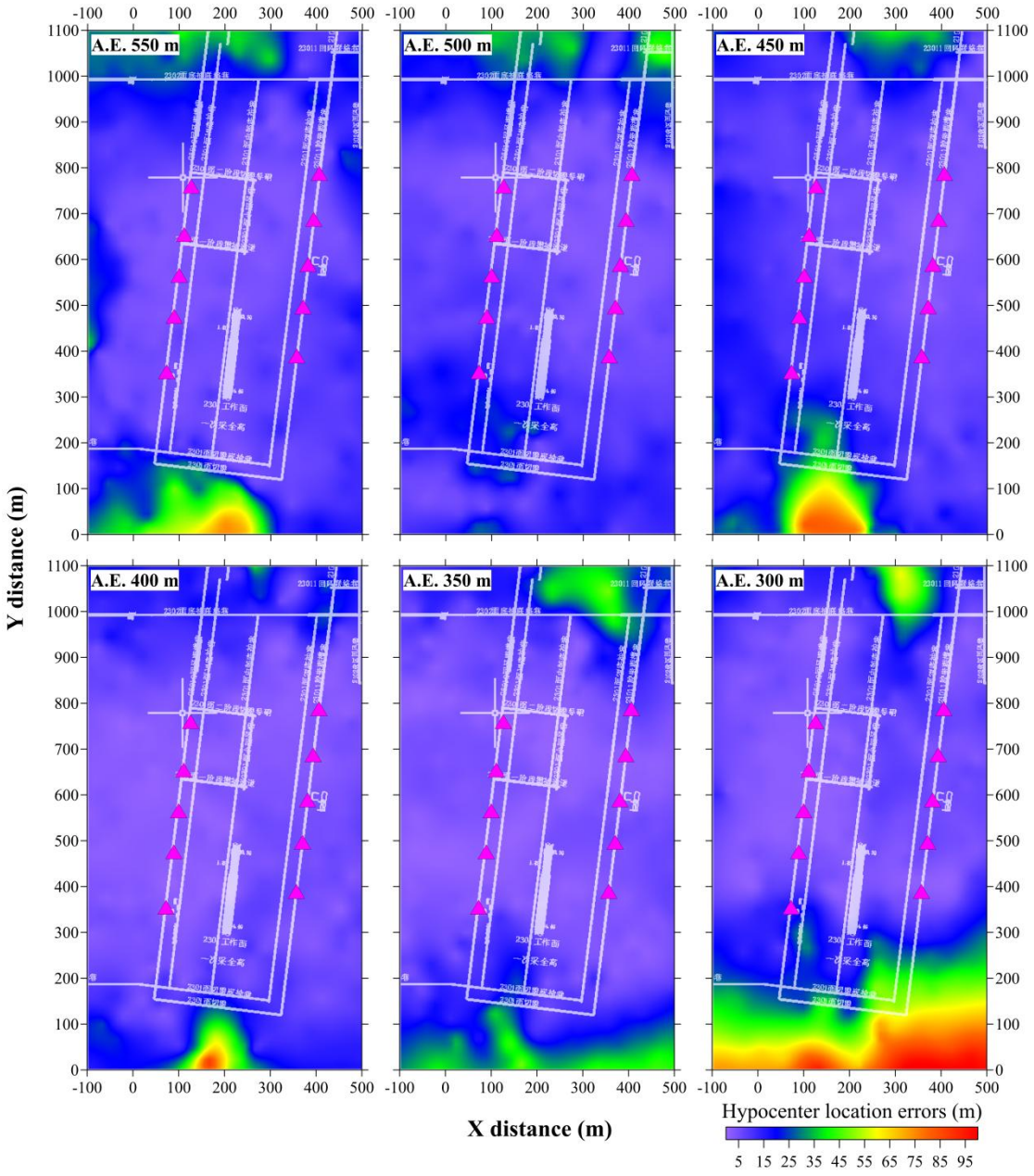


Figure 6. Location error contour maps of the 30,000 synthetic microseismic events. Red and blue colors denote high- and low-error regions, respectively. Purple triangles denote the ten KJ768 microseismic sensors deployed on 27 July, 2024. The elevations are annotated at the upper-left corner of each map.



296

297 **Figure 7. Same as Figure 6 but with a microseismic array deployed on 24 August, 2024.**

298

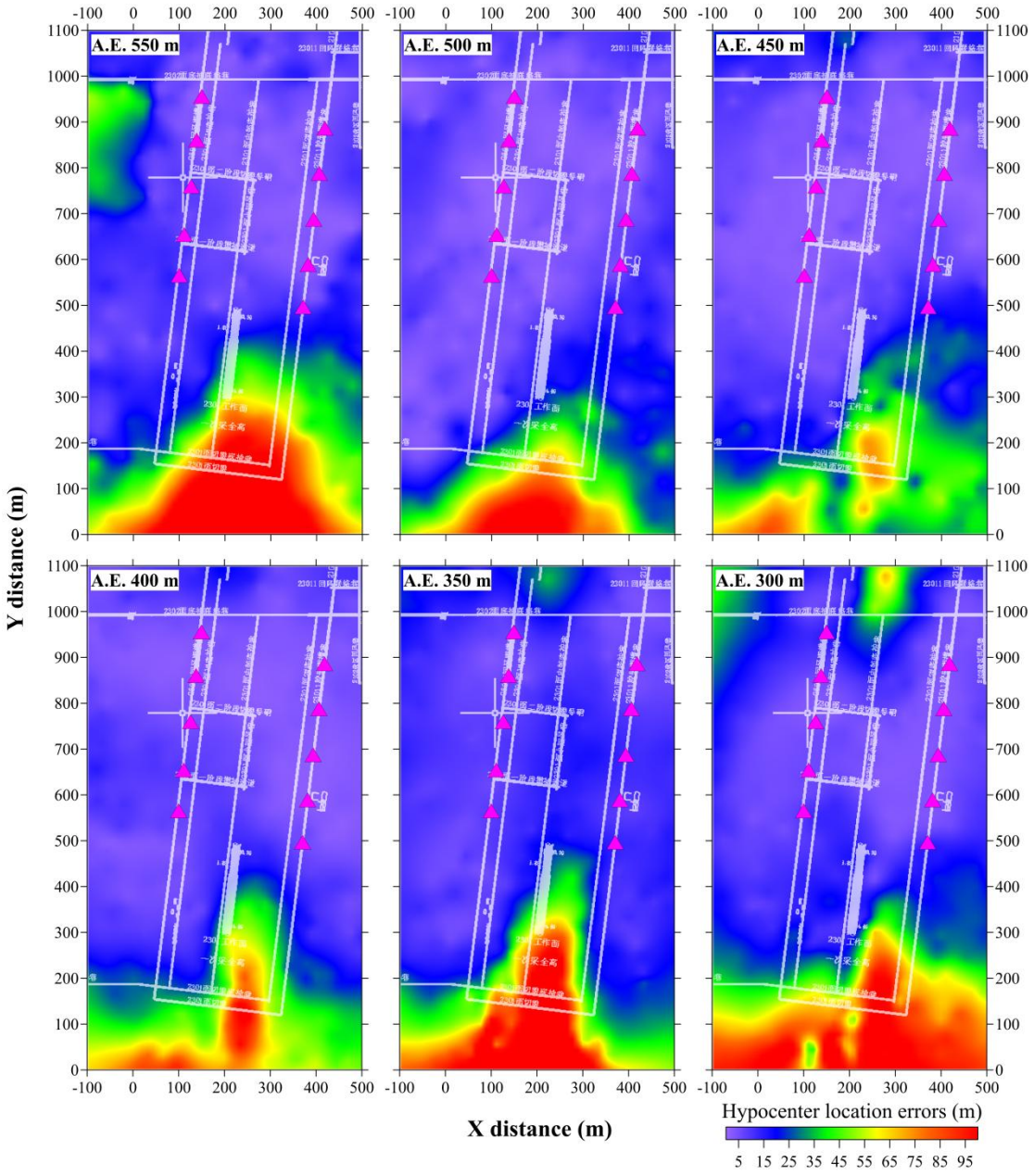


Figure 8. Same as Figure 6 but with a microseismic array deployed on 9 October, 2024.

(2) Location test in 3D Heterogeneous Media

To validate the effectiveness of the proposed precomputed travel-time grid interpolation technique in handling 3D heterogeneous velocity models, we further designed two types of regional grid velocity models: a layered model and a fully 3D heterogeneous model. The 3D model consists of a three-layer structure containing two anomalous zones—one with higher velocity and one with lower velocity. P-wave velocities of the three layers are 4.52 m/ms, 4.57 m/ms, and 4.61 m/ms, respectively, with the high-velocity anomaly having a velocity of 4.66 m/ms and the low-velocity anomaly of 4.48 m/ms (Fig. 9). Using the array geometry of 27 July 2024, the precomputed grid fields of theoretical travel-times and partial derivative coefficients over the entire volume are first calculated following the methodology described above. Subsequently, the theoretical travel-times for 500 synthetic events at an elevation of 450 m are

computed and used as "simulated" observational arrival-time data. Random perturbations uniformly distributed within [-5, +5] ms are added to the synthetic arrival-times. Source location inversion tests were then performed using the precomputed grid fields and the simulated observational data. To further examine the influence of velocity model bias on the location results, we also simulated a scenario in which the velocity model is biased: specifically, the precomputed grid fields are calculated using a homogeneous velocity model (v_p = 4.57 m/ms), whereas the simulated observational arrival-times are computed with the 3D heterogeneous model. The same inversion and location procedure is then applied. The contours of the location errors obtained from the three tests are shown in Fig. 10.

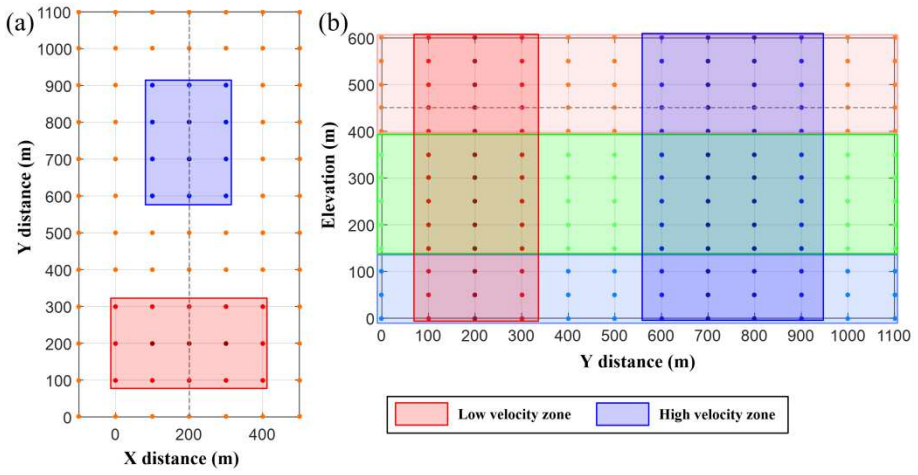


Figure 9. 3D heterogeneous grid model. The red and blue shaded regions denote low- and high-velocity zones, respectively, with velocities of 4.48 m/ms and 4.66 m/ms. The dashed black line in (b) marks an elevation of 450 m, where the synthetic events are located.

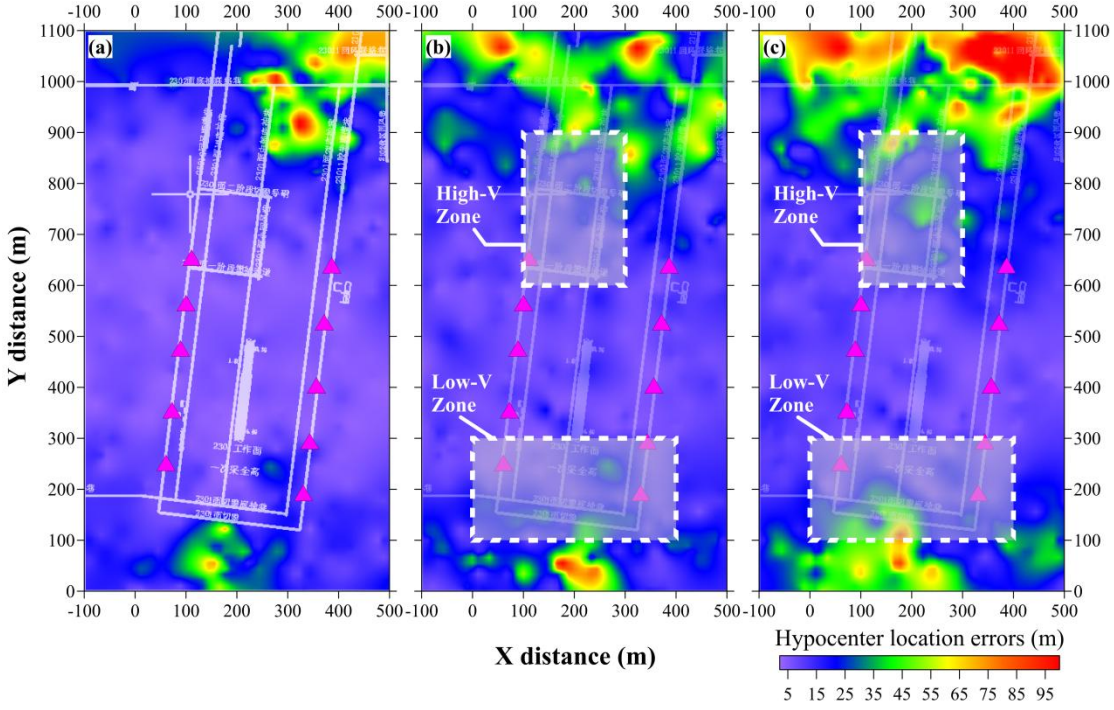


Figure 10. Location error contour maps at an elevation of 450 m obtained with three different velocity models. (a) Location result using a layered model. (b) Location result using the 3D heterogeneous model shown in Figure 9. (c) Same as (b), except that the precomputed grid

fields are calculated for a homogeneous velocity model. All other labels are the same as that in Figure 6.

The results show that the inversion under the 3D velocity model remains stable, similar to the homogeneous model case (Fig. 6, elevation 450 m), with a mean absolute location error of less than 5 m within the network coverage. Outside the network coverage, as the model complexity increases (Figs 6, 10a and 10b), the overall location accuracy declines slightly. This result indicates that under limited observational conditions, a complex regional velocity structure further aggravates the ill-conditioning of the misfit function, leading to greater inversion uncertainty. A comparison of Figs 10b and 10c shows that when the input model (i.e., the precomputed grid fields) deviates from the true subsurface structure (represented by the synthetic observational data), the location accuracy in the velocity anomaly zones (the high-V and low-V zones in Fig. 10c) deteriorates significantly. Nevertheless, within the network coverage, the location errors for most events can still be kept below ~10 m (Fig. 10c). This result demonstrates that when the observational geometry is reasonably complete, the proposed method leads to stable location results and exhibits low sensitivity to the velocity model bias. Therefore, when the velocity model is either complex or biased relative to the true structure, improving the completeness of the seismic monitoring network is a necessary measure for further enhancing location accuracy.

Locating real seismic events

The proposed method is applied to real microseismic monitoring data acquired from the No. 2301 working face of the Zhaozhuang Coal Mine, China. The array geometry employed is the same as that described above (Fig. 3). We manually identified microseismic events and picked arrival-times from three days of continuous raw waveform recordings—specifically, on 27 July, 24 August, and 9 October 2024. Guided by the methodology outlined above and an assessment of the signal-to-noise ratio of the field data, we select an arrival-time window length of 10 ms for the data input to the inversion (e.g. Fig. 11). Using a uniform-grid velocity model, we carry out a joint velocity and source inversion based on five blasting events conducted at this working face between 23 June and 4 July 2024, yielding an average P-wave velocity of ~4.57 m/ms for the coal seam in this region (Fig. S16).

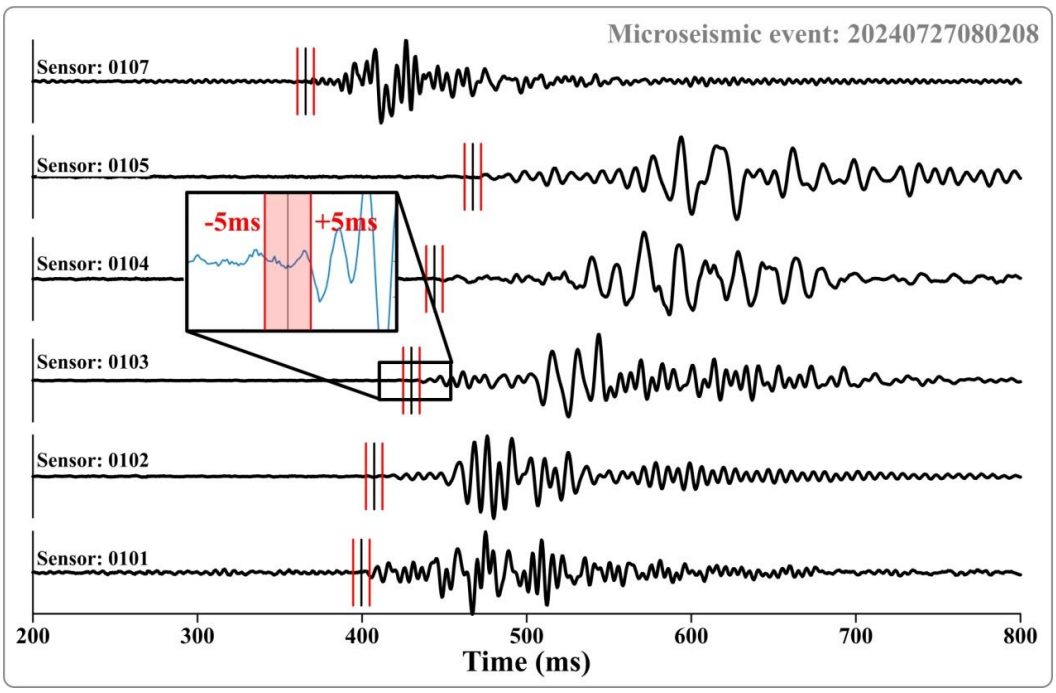


Figure 11. Example of arrival-time window selection for a real microseismic event.

Furthermore, the located events are selected according to the following criteria: (1) each event was recorded with clear P-wave arrivals by at least six sensors; (2) the event location lies within the study volume and sufficiently far from its boundaries; and (3) the mean residual of the least-squares inversion is less than 10 ms. As a result, 39 microseismic events are retained, and their epicentral distribution is shown in Fig.12.

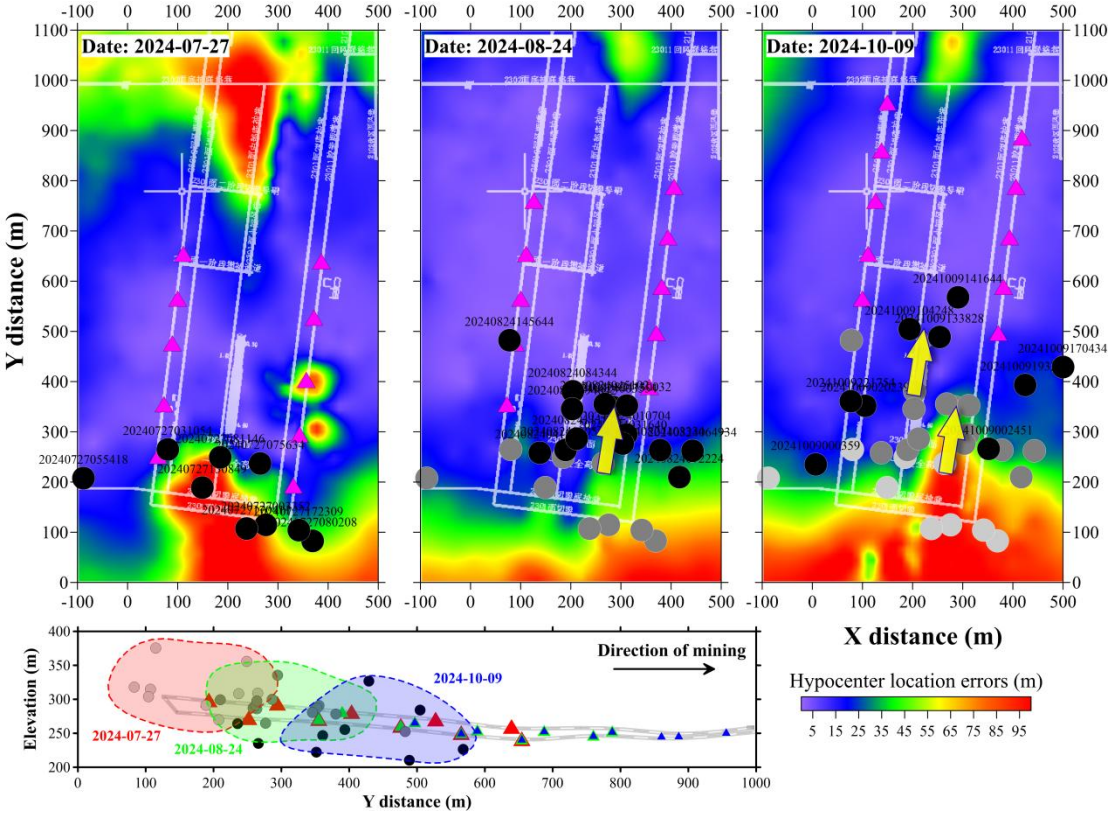


Figure 12. Location results of the selected microseismic events at the No. 2301 working face of the Zhaozhuang Coal Mine. Black dots in each map denote the events recorded by the array deployed on that day, with the deployment date annotated at the upper-left corner. The rainbow-colored basemap shows the theoretical location error contours at 300 m elevation obtained from synthetic tests. The lower inset displays the hypocenter distribution in a longitudinal cross-section along the gateway. The black arrow indicates the mining advance direction of the No. 2301 working face.

The vertical profile in Fig. 12 shows that the focal depths of the precisely located events are predominantly concentrated within about 100 m of the working face, indicating a close association with mining activities. The epicenters exhibit a distinct pattern of synchronous NNW ward migration in the direction of mining advance. This trend agrees well with previous results and established empirical findings[33–36], which in turn corroborates the overall reliability of our location method.

Discussion

Several limitations of the present method should be noted, and they point to directions for future improvement.

(1) Co-planar array geometry and the mirror-image problem

For a co-planar sensor array geometry, the inversion theoretically yields two symmetric solutions located on opposite sides of the network plane, which cannot be distinguished by the least-squares misfit alone. In our synthetic tests, we therefore imposed a priori constraints on the iterative inversion process by presetting the initial iteration direction to the side of the network plane where the true source resides. In the field data test, the majority of the finally retained microseismic events have focal depths concentrated around an elevation of ~300 m—that is, near the working face—suggesting that the mirror-image ambiguity has negligible impact in this case. Nevertheless, to fully resolve the mirror-image problem, adding sensors with vertical offset remains the most direct and effective solution. Furthermore, using the contour maps of location errors to determine an optimal network configuration that balances cost and location accuracy represents a valuable direction for future work.

(2) Efficiency of ray tracing in complex models

In this study, ray tracing is performed using a conventional shooting method combined with a finite-difference eikonal equation solver, which is computationally inefficient and struggles to handle models with complex velocity discontinuities. Integrating our inversion method with more efficient ray tracing techniques—such as the fast-marching upwind interpolation method[29] or the pseudo-bending-based fast ray tracing algorithm[30]—would represent a natural extension of the present approach.

(3) Sensitivity to outliers in observed data

Travel-time-based location methods are inherently sensitive to outliers in the observed data[37]. Although the proposed SDPR method effectively reduces the influence of data perturbations through its reformulation of the misfit function, a detailed quantitative analysis of how outliers with different statistical distributions affect the results is still lacking. Integrating the SDPR approach with location techniques designed to handle outliers—such as the principle behind the VFOM method[11]—would therefore represent another foreseeable and valuable research direction.

Conclusions

In this work, we have developed a new workflow for high-precision microseismic source location under limited observational conditions typical of mining environments. This workflow represents a further advancement and extension of the conventional travel-time-based location methods. Specifically, we propose a stochastic data perturbation regularization method, in which an arrival-time window, rather than a single pick, is used as the input, and a new travel-time misfit function is formulated based on stochastic process theory. This formulation reduces the high sensitivity of the inversion to data error perturbations that arise from the ill-conditioning of the governing equations. Furthermore, a precomputed travel-time grid interpolation technique is introduced to decouple the forward calculation from the inversion, thereby substantially improving the inversion efficiency and enabling rapid source location in complex 3D velocity models.

Synthetic tests demonstrate that, for observed arrival-time data containing error perturbations in a range of [-4, +4] ms, the proposed method achieves a single-event location time of 1–2 s and a location error of less than 5 m when the event lies inside the network coverage. For events located outside the network, the method still yields markedly more stable and convergent results than the conventional approach. Even for complex 3D velocity models, or when a velocity model bias exists, the proposed method still yields stable, high-accuracy locations within well-instrumented regions. Application of the method to real microseismic monitoring data from the Zhaozhuang Coal Mine shows that the precisely located epicenters exhibit a distinct pattern of synchronous northward migration with the advance of the mining face, which is consistent with previous findings. These results indicate that the proposed method provides an efficient and robust tool for microseismic source location in real mining environments, offering practical support for real-time hazard warning in coal mines.

Data availability

Data available on request from the corresponding author.

References

1. Xu, J. *Distribution Law of Mining-induced Strata Fractures and Its Applications*. China University of Mining and Technology Press, p422 (2016).
2. Li, N., Wang, E. & Ge, M. Microseismic monitoring technique and its applications at coal mines: present status and future prospects. *Journal of China Coal Society* **42**, 83–96 (2017).
3. Geiger, L. Herdbestimmung bei erdbeben aus den ankunftszeiten. K. *Gesell. Wiss. Gott.* **4**, 331–349 (1910).
4. Li, L., Tan, J., Schwarz, B., Staněk, F., Poiata, N., Shi, P., et al. Recent advances and challenges of waveform-based seismic location methods at multiple scales. *Reviews of Geophysics* **58**, e2019RG000667 (2020).
5. Cheng, J., Song, G., Sun, X., Wen, L. & Li, F. Research developments and prospects on microseismic source location in mines. *Engineering* **4**, 653–660 (2018).
6. Xu, L., Du, H., Yan, C. & Li, C. A method for determination of earthquake hypocentroid: time-reversal imaging technique I—principle and numerical tests. *Chinese Journal of Geophysics* **56**, 1190–1206 (2013). (Chinese)
7. Gu, M. Elastic wave time-reversal source imaging. Hefei: University of Science and

Technology of China, (2016). (Chinese)
8. Swanson, P., Estey, L., Boler, F. & Billington, S. *Accuracy and Precision of Microseismic Event Locations in Rock Burst Research Studies*. Washington, D.C.: U.S. Dept. of the Interior, Bureau of Mines, p40 (1992).
9. Li, N. Research on mechanisms of key factors and reliability for microseismic source location. China University of Mining & Technology, (2014). (Chinese)
10. Hu, J. & Li, S. Optimization of picking mine microseismic P-wave arrival time and its application in reducing error of source locating. *Chinese Journal of Geotechnical Engineering* **36**, 1940–1946 (2014). (Chinese)
11. Li, X.B., Wang, Z.W. & Dong, L.J. Locating single-point sources from arrival times containing large picking errors (LPEs): the virtual field optimization method (VFOM). *Scientific Reports* **6**, 19205 (2016).
12. Zeng, Z., Han, P., et al. An Adaptive Probabilistic Imaging Location Method for Microseismic Monitoring. *IEEE Transactions on Geoscience and Remote Sensing* **63**, 1–16 (2025).
13. Tikhonov, A.N. & Arsenin, V.Y. *Solution of ill-posed problems*. Winston, Wiley, New York, (1977).
14. Hohenester, U., Rekdal, P.K., Borzi, A. & Schmiedmayer, J. Optimal quantum control of Bose-Einstein condensates in magnetic microtraps. *Physical Review A* **75**, 023602 (2007).
15. Hintermuller, M., Marahrens, D., Markowich, P.A. & Sparber, C. Optimal bilinear control of Gross-Pitaevskii equations. *Society for Industrial and Applied Mathematics Journal on Control and Optimization* **51**, 2509–2543 (2013).
16. Mennemann, J., Matthes, D., Weishaupl, R. & Langen, T. Optimal control of Bose-Einstein condensates in three dimensions. *New Journal of Physics* **17**, 113027 (2015).
17. Adriazola, J. & Goodman, R.H. Optimal control approach to gradient-index design for beam reshaping. *Journal of the Optical Society of America A* **39**, 907 (2022).
18. Adriazola, J. & Goodman, R.H. Reduction-based strategy for optimal control of bose-einstein condensates. *Physical Review E* **105**, 025311 (2022).
19. Wishart, J. The Generalised Product Moment Distribution in Samples from a Normal, Multivariate Population. *Biometrika* **20**, 32–52 (1928).
20. Couillet, R. & Liao, Z. *Random Matrix Methods for Machine Learning*. Cambridge University Press, (2022).
21. Franklin, J.N. Well-posed stochastic extensions of ill-posed linear problems. *Journal of Mathematical Analysis and Applications* **31**, 682–716 (1970).
22. Tarantola, A. Inverse Problem *Theory and Methods for Model Parameter Estimation*. Society for Industrial and Applied Mathematics, p342 (2005).
23. Jia, B.X., Zhao P., Jiang, M., et al. Three-dimensional propagation model building in heterogeneous medium of mine earthquake shock wave and its application. *Journal of China Coal Society* **39**, 364–370 (2014). (Chinese)
24. Zhou, L.L., Jia, B.X., Pan, Y.S., et al. Wave velocity model and microseismic location method of goaf overburden rock. *Journal of China Coal Society* **48**, 2049–2064 (2023). (Chinese)
25. Stewart, G.W. The decompositional approach to matrix computation. *Computing in Science & Engineering* **2**, 50–59 (2000).
26. Draper, N.R. & Smith, H. *Applied Regression Analysis (Second Edition)*. John Wiley & Sons, Inc., p709 (1981).

27. Broyden, C.G. Quasi-Newton methods and their application to function minimisation. *Mathematics of Computation* **21**, 368–381 (1967).
28. Julian, B.R. *Ray tracing in arbitrarily heterogeneous media*. Tech.Note, 45, Lincoln Lab., Lexington, Mass., (1970).
29. Jiang, R., Xu, N., Feng, D. & Zhou J. Research on microseismic location based on fast marching upwind linear interpolation method. *Rock and soil mechanics* **40**, 3697–3708 (2019).
30. Um, J. & Thurber, C. A fast algorithm for two-point seismic ray tracing. *Bulletin of the Seismological Society of America* **77**, 972–986 (1987).
31. Asakawa, E., & Kawanaka, T. Seismic ray tracing using linear traveltime interpolation. *Geophysical Prospecting* **41**, 99–111 (1993).
32. Zhang, G., Deng, Z., Jiang, J. & An, Y. Application of KJ768 Micro-seismic monitoring system in early warning of strong mine pressure disaster in high gassy mines. *Meikuang Anquan* **51**, 144–147 (2020).
33. Reginald, H.H. & Mowrey, G.L. Study of microseismic activity associated with a longwall coal mining operation using a near-surface array. *Engineering Geology* **10**, 263–281 (1976).
34. Andrzej, L. & Zbigniew, I. Space–time clustering of seismic events and hazard assessment in the Zabrze-Bielszowice coal mine, Poland. *International Journal of Rock Mechanics and Mining Sciences* **46**, 918–928 (2009).
35. James, P.V., Kendall, J., Antony B., Richard L. & Brian J. Seismicity induced by longwall coal mining at the Thoresby Colliery, Nottinghamshire, U.K. *Geophysical Journal International* **212**, 942–954 (2018).
36. Ghosh, G.K. & Sivakumar, C. Application of underground microseismic monitoring for ground failure and secure longwall coal mining operation: A case study in an Indian mine. *Journal of Applied Geophysics* **150**, 21–39 (2018).
37. Pesicek, J.D., Child, D., Artman, B. & Cieslik, K. Picking versus stacking in a modern microearthquake location: Comparison of results from a surface passive seismic monitoring array in Oklahoma. *Geophysics* **79**, KS61–KS68 (2014).

Acknowledgements

We thank Jinneng Holding Equipment Manufacturing Group, China, for providing the microseismic waveform data used in this study.

Author contributions

Conceptualization, R.J. and H.Q.; Methodology, R.J. and D.P.Z.; Software, R.J.; Validation, R.J., H.Q. and W.L.; Investigation, R.J., Y.G.L., K.Q. and Y.X.; Writing-Original Draft Preparation, R.J.; Writing-Review & Editing, D.P.Z. and R.J.; Project administration, H.Q. and W.L.; Funding acquisition, H.Q.

Funding

This research was jointly supported by the National Natural Science Foundation of China (Grant No. 52574247), and the Science and Technology Development Foundation of the China Coal Reasearch Institude (Grant Nos. 2025CG-AQ-03 and 2024ZDI-06).

Declarations

Competing interests

The authors declare no competing interests.

Additional information

Supplementary data to this article can be found online. Correspondence and requests for materials should be addressed to H.Q.

Supplementary Files

This is a list of supplementary files associated with this preprint. Click to download.

- SIJiaMicroseismiclocation20260518.docx